Journal of Sound and Vibration (1996) **191**(1), 75–90

STRUCTURE-BORNE SOUND TRANSMISSION BETWEEN THIN ORTHOTROPIC PLATES: ANALYTICAL SOLUTIONS

I. Bosmans, P. Mees and G. Vermeir

Laboratory for Building Physics, Department of Civil Engineering, Catholic University of Leuven, Celestijnenlaan 131, *B*-3001 *Leuwen* (*Heverlee*), *Belgium*

(*Received* 12 *September* 1994, *and in final form* 13 *February* 1995)

Two models are presented for predicting structure-borne sound transmission between thin orthotropic plates connected by a rigid junction. The first is based on a solution for the wave propagation in semi-infinite plates, and the second is based on a modal summation solution for finite-sized plates. Numerical results for the bending wave transmission across an L-junction demonstrate the inherent similarities and differences of both models. Results for a junction of orthotropic plates are compared with results for an equivalent junction of isotropic plates. The use of an orthotropic plate model in the context of an SEA method is discussed.

1. INTRODUCTION

The calculation of the vibrational energy transmission at a junction between plates is an important subject in the prediction of structure-borne sound transmission in buildings. Solutions of this problem have been reported in the literature for various types of junctions, obtained by using different theoretical models.

With regard to theoretical models, one can distinguish between calculation methods for semi-infinite and finite-sized plates. Both methods are based on a proper formulation of the continuity and equilibrium conditions at the junction between the plates, but different formulations are used for the plate displacements and the structure-borne sound excitation. For semi-infinite plates, displacements are expressed as bending and in-plane longitudinal and transverse waves propagating in the structure. The energy flow at the junction is quantified by the reflection and transmission coefficients, which are defined as the ratios of the reflected and transmitted intensities, respectively, to the intensity carried by an incident wave. For finite-sized plates, displacements are usually expressed as modal summations. The energy flow at the junction or the average plate displacements are calculated for concentrated or randomly positioned point force excitation. For restricted cases, analytical solutions are available [1, 2], but numerical solutions by the finite element method have also been reported [3, 4].

With regard to the type of junctions and plates, one can distinguish between geometries with varying complexity. The standard case of sound transmission at a rigid junction has been solved both for thin and thick (Mindlin) plates [5]. The case of a junction with a rigid beam has been treated by Langley and Heron [6]. The case of junctions with an elastic

0022–460X/96/110075+16 $18.00/0

interlayer has been studied by Cremer *et al*. [7], Wöhle *et al*. [8, 9] and more recently by Mees and Vermeir [10, 11].

This paper presents an extension of theoretical models for structure-borne sound transmission at rigid junctions between isotropic plates towards the case of junctions between orthotropic plates. The study is inspired by the observation that many floor constructions in buildings are orthotropic up to a certain degree by virtue of their internal structure. The use of precast hollow elements can lead to a ratio of the bending stiffness in two mutual perpendicular directions of 1·4. For the case of a floor plate with stiffeners this ratio can easily reach 10. The principal aim of the study is to quantify the effect of orthotropic plate characteristics on the vibration transmission at junctions, to demonstrate the difference and similarity between models for orthotropic and isotropic plates, and to discuss the use of the models in the context of an SEA calculation scheme.

The paper is organized as follows. First, the equations of motion governing wave propagation in orthotropic plates are reviewed. Elementary solutions for the wave propagation are discussed, emphasizing differences with the isotropic case. In the second part, the elementary solutions are applied to the calculation of structure-borne sound transmission at junctions, both for the case of semi-infinite and finite-sized plates. Next, the elements crucial to a proper implementation of the orthotropic plate model in an SEA scheme are discussed. Finally, the principal characteristics of the models are demonstrated by numerical results for an L-junction with varying plate dimensions and varying orthotropic stiffness of the plate material.

2. EQUATIONS OF MOTION AND WAVE PROPAGATION IN ORTHOTROPIC PLATES

The study is restricted to elastic, orthotropic plates with a small thickness compared to the bending wavelength. It is assumed that orthotropic plate characteristics result from elastic properties of the plate material and not from the plate geometry or internal structure: consequently, the plates are assumed to be homogeneous. The thin plate assumption implies a plane stress state, given by the following stress–strain relations expressed in a co-ordinate system parallel to the principal material directions, with the z-axis perpendicular to the plate surface [12] (a list of symbols is presented in the Appendix):

$$\begin{bmatrix} \sigma_x \\ \sigma_y \\ \tau_{xy} \end{bmatrix} = \begin{bmatrix} E'_x & \nu_{yx}E'_x & 0 \\ \nu_{xy}E'_y & E'_y & 0 \\ 0 & 0 & G_{xy} \end{bmatrix} \begin{bmatrix} \epsilon_x \\ \epsilon_y \\ \gamma_{xy} \end{bmatrix}. \tag{1}$$

Here

$$E'_{x,\,y} = E_{x,\,y}/(1-\nu_{xy}\nu_{yx}). \tag{2}$$

Given the condition of symmetry of the stiffnesses, $\nu_{xy}E_y = \nu_{yx}E_x$, four independent constants are required to characterize the plate material: E_x, E_y, G_{xy} and ν_{xy}.

The classical thin plate kinematic assumptions and the orthotropic stress–strain relations result in uncoupled equations of motion for the transverse (bending) displacement ζ and the in-plane displacements ξ and η, respectively:

$$B_x\,\partial^4\zeta/\partial x^4 + 2(\nu_{xy}B_y + 2G)\,\partial^4\zeta/\partial x^2\,\partial y^2 + B_y\,\partial^4\zeta/\partial y^4 + \rho h\,\partial^2\zeta/\partial t^2 = 0. \tag{3}$$

Here

$$B_{x,y} = E'_{x,y} h^3/12, \qquad G = G_{xy} h^3/12, \tag{4}$$

$$E'_x h\, \partial^2\xi/\partial x^2 + \nu_{yx} E'_x h\, \partial^2\eta/\partial x\, \partial y + G_{xy} h(\partial^2\xi/\partial y^2 + \partial^2\eta/\partial x\, \partial y) - \rho h\, \partial^2\xi/\partial t^2 = 0, \tag{5}$$

$$G_{xy} h(\partial^2\xi/\partial x\, \partial y + \partial^2\eta/\partial x^2) + E'_y h\, \partial^2\eta/\partial y^2 + \nu_{xy} E'_y h\, \partial^2\xi/\partial x\, \partial y - \rho h\, \partial^2\eta/\partial t^2 = 0. \tag{6}$$

In the thin plate bending wave equation (3) the influences of rotary inertia and transverse shear are neglected. This approximation is valid only when the thickness of the plate is small compared to the bending wavelength [7]. Although floors and walls cannot be regarded as thin over the whole frequency range of interest in building acoustics, it is assumed that equation (3) can be used to study the effect of orthotropy on the sound transmission at junctions. Cremer *et al*. [7] proposed an identical equation of motion for ribbed and corrugated plates, provided that the bending wavelength is considerably greater than the rib or corrugation spacing.

Unlike the corresponding equations for isotropic plates, equations (5) and (6) cannot be separated into uncoupled equations for purely in-plane quasi-longitudinal and shear wave motion. This corresponds to the physical reality that in an orthotropic material, in a direction different from the principal material directions, compression (or tension) always induces in-plane shear.

Elementary solutions of equations (3), (5) and (6) consist of determining the wavenumbers for plane wave propagation in an infinitely extended plate. These solutions are used to set up equations for the sound transmission at junctions between plates.

A solution for the displacement ζ of a plane harmonic bending wave propagating in a direction characterized by an angle θ with the first principal direction is written as

$$\zeta(x, y, t) = A\, \mathrm{e}^{-\mathrm{j}k_b \cos\theta\, x}\, \mathrm{e}^{-\mathrm{j}k_b \sin\theta\, y}\, \mathrm{e}^{\mathrm{i}\omega t}. \tag{7}$$

The bending wavenumber k_b is determined by substitution of equation (7) in equation (3),

$$k_b(\theta) = \sqrt{\omega}\sqrt[4]{\rho h/B(\theta)}, \tag{8}$$

where the bending stiffness $B(\theta)$ is given by

$$B(\theta) = (h^3/12)(E'_x \cos^4\theta + 2(\nu_{xy} E'_y + 2G_{xy}) \cos^2\theta \sin^2\theta + E'_y \sin^4\theta). \tag{9}$$

Expression (9) reveals some important facts. Except for the correction for the plane stress condition $(1 - \nu_{xy}\nu_{yx})$, an orthotropic plate behaves completely like an isotropic plate for the case of a plane bending wave propagating in the principal material directions. For all other angles, however, the shear constant G_{xy} influences the bending wavenumber. This can be explained by the fact that due to the difference between the Young's moduli in the principal directions, compression (or tension) will induce in-plane shear, as illustrated in Figure 1. Since bending induces in-plane normal stresses, the bending stiffness in an arbitrary direction θ will also depend on the shear modulus G_{xy} of the plate material. Figure 2 shows the bending wavenumber as a function of the angle of propagation for three values of G_{xy}.

The displacements ξ and η of a plane harmonic in-plane wave propagating in a direction characterized by an angle θ with the first principal direction are written as

$$\xi(x, y) = A\, \mathrm{e}^{-\mathrm{j}k_p \cos\theta\, x}\, \mathrm{e}^{-\mathrm{j}k_p \sin\theta\, y}, \qquad \eta(x, y) = VA\, \mathrm{e}^{-\mathrm{j}k_p \cos\theta\, x}\, \mathrm{e}^{-\mathrm{j}k_p \sin\theta\, y}, \tag{10, 11}$$

where V is the ratio between the amplitudes of the in-plane displacements η to ξ. Substitution in the equations of motion results in two wavenumbers, corresponding to

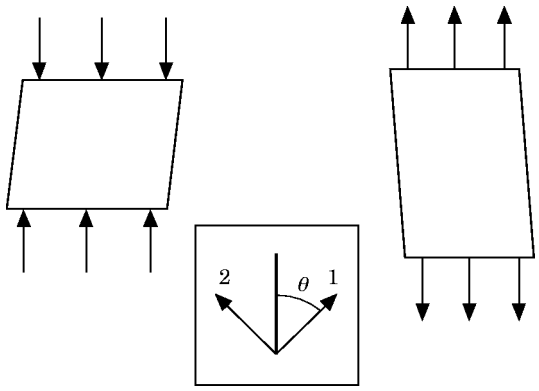

Figure 1. Applying compressive or tensile stress on the edges of an orthotropic plate in a direction other than the principal directions results in a shear deformation.

two different wave types, each characterized by a different value of V. The in-plane translation ratios $V_{1,2}$ are calculated as the roots of the quadratic equation

$$aV^2+bV+c=0, \tag{12}$$

where

$$a=(v_{yx}E'_x+G_{xy})\cos\theta\,\sin\theta,$$
$$b=E'_x\cos^2\theta-E'_y\sin^2\theta+G_{xy}(\sin^2\theta-\cos^2\theta), \qquad c=-a. \tag{13}$$

Finally, the in-plane wavenumbers are given by

$$k_{p1,2}(\theta)=\omega\sqrt{\rho/\{E'_x\cos^2\theta+G_{xy}\sin^2\theta+(v_{xy}E'_y+G_{xy})\cos\theta\,\sin\theta\,V_{1,2}(\theta)\}}. \tag{14}$$

Figure 3 shows the in-plane wavenumbers as functions of the propagation direction. Again, for the case of in-plane wave propagation in the principal directions, orthotropic plates behave exactly like isotropic ones. For this case only, the equations of motion (5)

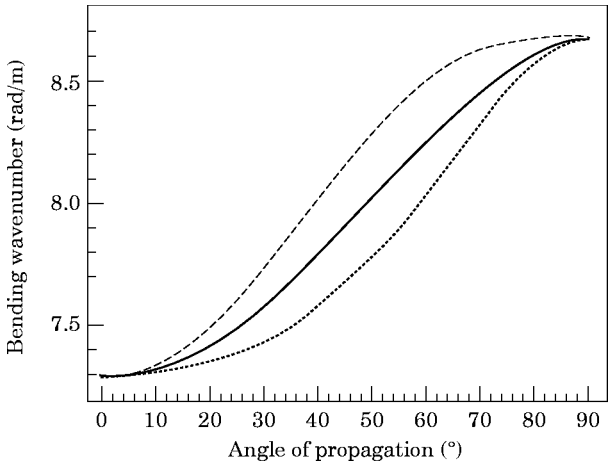

Figure 2. Bending wavenumber at 1000 Hz for a thin orthotropic plate as a function of the angle of propagation, for three different values of the shear modulus G_{12}. Material properties: $E_1=4{\cdot}0\times10^{10}$ Pa, $E_2=2{\cdot}0\times10^{10}$ Pa, $v_{12}=0{\cdot}3$, $\rho=2500$ kg/m^3 and $G_{12}=1{\cdot}538\times10^{10}$ Pa (· · · ·), $G_{12}=1{\cdot}154\times10^{10}$ Pa (——), $G_{12}=7{\cdot}692\times10^{9}$ Pa (- - - -).

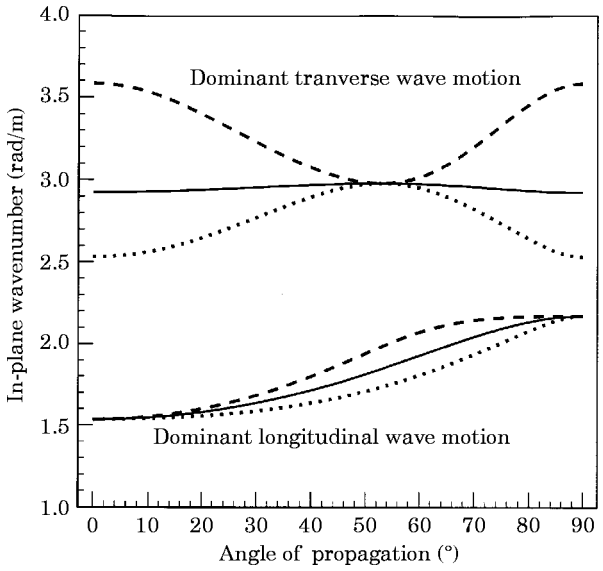

Figure 3. In-plane wavenumber at 1000 Hz for a thin orthotropic plate as a function of the angle of propagation, for three different values of the shear modulus G_{12}. Material properties: $E_1 = 4{\cdot}0 \times 10^{10}$ Pa, $E_2 = 2{\cdot}0 \times 10^{10}$ Pa, $\nu_{12} = 0{\cdot}3$, $\rho = 2500$ kg/m^3 and $G_{12} = 1{\cdot}538 \times 10^{10}$ Pa (· · · · ·), $G_{12} = 1{\cdot}154 \times 10^{10}$ Pa (——), $G_{12} = 7{\cdot}692 \times 10^9$ Pa (- - - -).

and (6) are uncoupled, resulting in pure in-plane quasi-longitudinal and transverse wave motion. For all other directions both wave types are characterized by a mixture of longitudinal and transverse motion. However, it is shown in Figure 3 that both wave types can be regarded as predominantly longitudinal or predominantly transverse.

3. STRUCTURE-BORNE SOUND TRANSMISSION BETWEEN ORTHOTROPIC PLATES

The model of the plate junction is shown in Figure 4. The junction consists of an assembly of orthotropic plates connected by means of a massless and perfectly flexible beam, which is not restricted with respect to its translation. Both the local co-ordinate system and the plate edges are parallel to the principal material directions of the plates. Structure-borne sound excitation is applied to plate 1. The response of the plate assembly and the resulting energy flow through the junction follow from the equilibrium and the continuity conditions at the junction. Material damping was included only in the model for finite plates and not in the wave analysis for the case of semi-infinite plates.

For a junction between semi-infinite plates, the analysis is performed by using the wave approach as reported by Wöhle *et al*. [8, 9] and by Craven and Gibbs [13, 14]. The structure-borne sound excitation is modelled as a wave incident on the plate junction. This wave generates bending- and in-plane waves propagating away from the junction on all plates, with identical spatial dependencies along the y-axis as imposed by the incident wave. The plate displacements ξ_p, η_p, ζ_p and α_p are governed by the solutions of the equations of motion (3), (5) and (6). The displacements as well as the forces are expressed on the plate edges, where the forces are derived from the displacements using the elementary formulae of mechanics. The equilibrium and continuity conditions at the junction line lead to a set of linear equations, the solution of which yields the complex displacement amplitudes of the plates and the junction beam. The bending wave transmission coefficient τ_{1p} from plate 1 to plate p is defined as the ratio of the transmitted

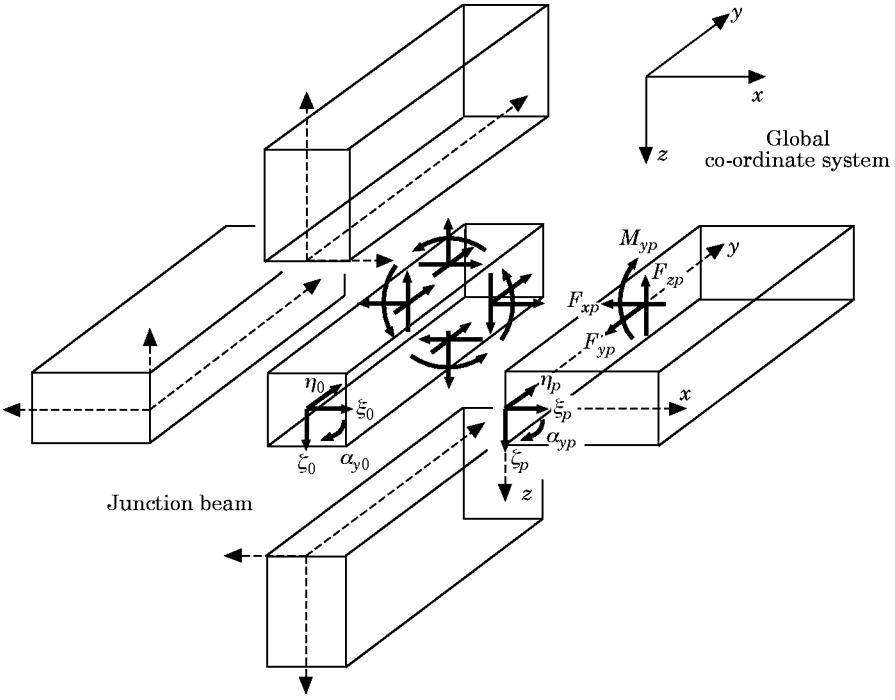

Figure 4. Model of the plate junction.

to the incident bending wave intensity normal to the junction line, for a given angle of incidence and for a given frequency:

$$\tau_{1p}(\theta) = I_{x1p}(\theta)/I_{x1}(\theta). \tag{15}$$

The average transmission coefficient $\bar{\tau}_p$ for random incidence is calculated by an integration over all the angles of incidence. Finally, the bending wave transmission loss R_p is calculated as

$$R_p = -10 \log(\bar{\tau}_p). \tag{16}$$

For a junction between finite plates, the analysis is performed by using a modal summation technique, as reported by Cuschieri [15] and Mees and Vermeir [11]. A harmonic point force is located on the source plates, and the bending- and in-plane wave fields are expressed as series expansions in the direction parallel to the junction line, assuming simply supported boundary conditions. The boundary condition at the edges parallel to the junction line can be chosen freely. The solution to the equations of motion (3), (5) and (6) can be written as

$$\zeta(x, y) = \sum_n (e^{k_{bn1}x} A_n + e^{-k_{bn1}x} B_n + e^{k_{bn2}x} C_n + e^{-k_{bn2}x} D_n) \sin\left(\frac{n\pi}{L_y} y\right), \tag{17}$$

$$\xi(x, y) = \sum_n (e^{k_{pn1}x} A'_n + e^{-k_{pn1}x} B'_n + e^{k_{pn2}x} C'_n + e^{-k_{pn2}x} D'_n) \sin\left(\frac{n\pi}{L_y} y\right), \tag{18}$$

$$\eta(x, y) = \sum_n (V_{n1} e^{k_{pn1}x} A'_n - V_{n1} e^{-k_{pn1}x} B'_n + V_{n2} e^{k_{pn2}x} C'_n - V_{n2} e^{-k_{pn2}x} D'_n) \cos\left(\frac{n\pi}{L_y} y\right) \tag{19}$$

where the harmonic time dependence $e^{j\omega t}$ has been omitted.

The eigenmode amplitudes and the displacement amplitudes of the junction beam are the unknowns of the problem. Forces and displacements are expressed as modal summations at the plate edges parallel to the junction line. The equilibrium and continuity conditions at the junction line, and the boundary conditions at the free plate edges result in a set of linear equations, the solution of which yields the unknown modal amplitudes. From these, the root mean square transverse velocities $\langle \dot{\zeta}(x, y) \rangle^2$ of all the plates are calculated. Finally, the bending wave transmission between plate 1 and plate p is quantified by the root mean square velocity level difference L_{vp}:

$$L_{vp} = 10 \log (\langle \dot{\zeta}_1 \rangle^2 / \langle \dot{\zeta}_p \rangle^2). \tag{20}$$

4. STATISTICAL ENERGY ANALYSIS FOR ORTHOTROPIC PLATES

The statistical energy analysis (SEA), based on the work of Lyon [16], is a framework for evaluating the vibrational energy distribution in a complex structure. The problem of the energy distribution is solved by dividing the structure into coupled subsystems and subsequently writing the energy balance of each subsystem. Two important parameters in an SEA model are the coupling loss factor between two coupled subsystems and the modal density of a subsystem. In this section both parameters will be derived for subsystems associated with the bending wave field on an orthotropic plate. Similar calculations can be made for subsystems associated with both in-plane wave types on a thin orthotropic plate and will therefore not be presented here.

4.1. COUPLING LOSS FACTOR

Consider a junction of two orthotropic, finite-sized plates i and j. The junction line is parallel to the y-axis. When plate i is excited, energy flows from plate i to plate j resulting in a reverberant bending wave field on both plates. In the SEA method, this energy flow Π_{ij} is expressed as a function of the total kinetic energy E_{ki} of the source plate and the coupling loss factor η_{ij}:

$$\Pi_{ij} = E_{ki} \omega \eta_{ij}. \tag{21}$$

For structural coupling between two subsystems, the coupling loss factor η_{ij} is usually calculated from a wave analysis of the coupling between two corresponding semi-infinite subsystems. A reverberant bending wave field on a finite-sized plate, for example, is modelled by bending waves propagating in arbitrary directions on a corresponding infinite plate. The energy flow Π_{ij} between two plates is obtained by averaging the individual contributions of all bending waves randomly incident on a junction of semi-infinite plates. For coupling between isotropic plates, the following expression for the energy flow can be derived [16]:

$$\Pi_{ij} = \frac{E_{di} C_{gi} l_{ij}}{2\pi} \int_{-\pi/2}^{\pi/2} \tau_{ij}(\theta) \cos \theta \, \mathrm{d}\theta. \tag{22}$$

Here E_{di} is the energy per unit area, C_{gi} is the group velocity for bending waves, and l_{ij} is the length of the plate junction. τ_{ij} is the angle dependent transmission coefficient of the junction as defined by equation (15). Combination of equations (21) and (22) yields a relation between the coupling loss factor and the average transmission coefficient.

When applying this procedure to bending wave transmission between orthotropic plates, two elements have to be considered: the power distribution over all angles of incidence in a reverberant field, and the propagation direction of the bending wave energy.

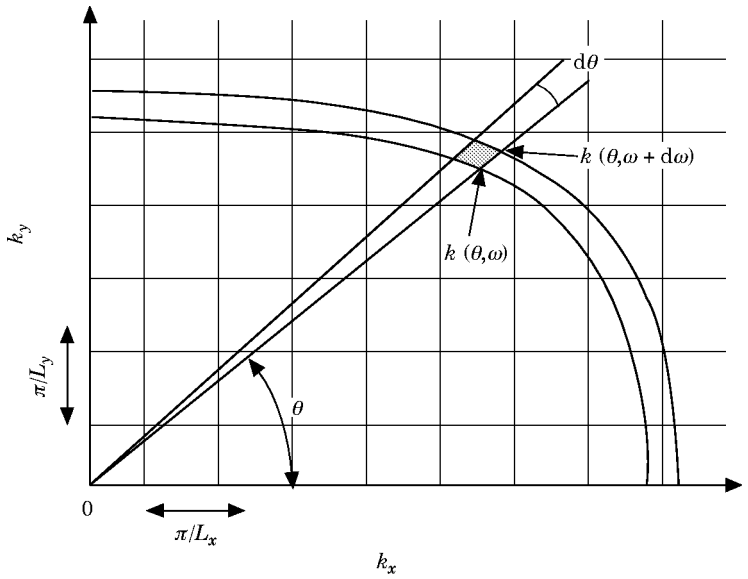

Figure 5. Modal lattice of an orthotropic plate showing the bending wavenumber as a function of the propagation direction. The distribution of the energy flow in a diffuse wave field is determined by the distribution of the area in the interval $k(\theta, \omega)$ and $k(\theta, \omega+\mathrm{d}\omega)$.

In a diffuse wave field on an orthotropic plate the energy is not distributed uniformly among the various directions of propagation. Lyon [16] derived a weighting function $D(\theta)$ that quantifies this energy distribution by considering the area in the interval $k(\theta, \omega)$ and $k(\theta, \omega+\mathrm{d}\omega)$ measured in the wavenumber diagram as shown in Figure 5. For the case of orthotropic plates this procedure results in the weighting function

$$D(\theta) = C/\sqrt{E(\theta)}, \tag{23}$$

where the constant C is derived from the condition

$$\int_0^{2\pi} D(\theta)\,\mathrm{d}\theta = 2\pi. \tag{24}$$

In bending wave propagation on an orthotropic plate, energy travels in a direction different from that of the bending wave causing the energy flow. The intensities in the principal directions for a bending wave with unit amplitude travelling in a direction θ are given by

$$I_x(\theta) = \omega k_b^3 B_x(\cos^2\theta + (\nu_{yx} + 2G_{xy}/E_x')\sin^2\theta)\cos\theta, \tag{25}$$

$$I_y(\theta) = \omega k_b^3 B_y(\sin^2\theta + (\nu_{xy} + 2G_{xy}/E_y')\cos^2\theta)\sin\theta. \tag{26}$$

Figure 6 shows the angle of the intensity vector as a function of the direction of propagation for five ratios of E_y to E_x. It is clearly illustrated that the direction of the intensity deviates towards the stiffest principal direction.

By combining the expressions for the energy distribution and propagation direction, it is now possible to derive an expression for the intensity incident on the junction, carried by a bending wave with unit amplitude, travelling in an elementary interval $(\theta, \theta+\mathrm{d}\theta)$ on plate i:

$$\mathrm{d}I_x = I_{xi}(\theta)D_i(\theta)\,\mathrm{d}\theta/2\pi \tag{27}$$

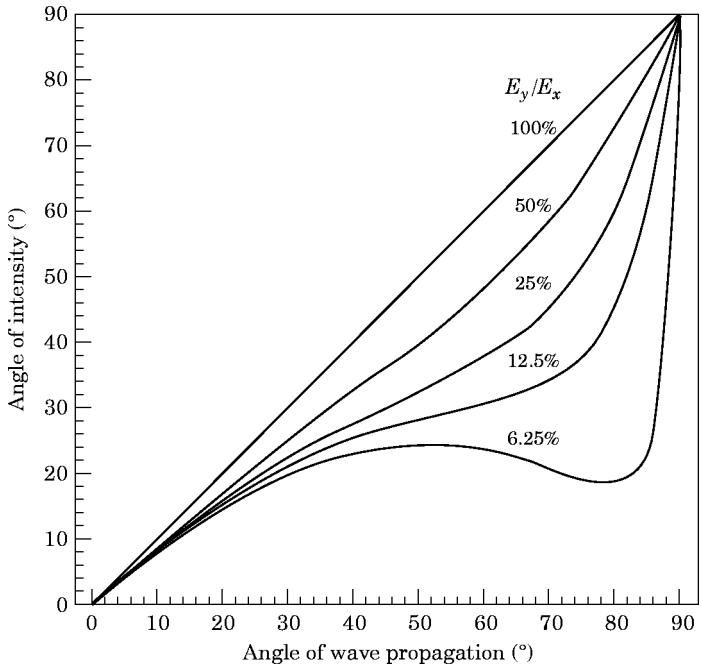

Figure 6. Direction of the energy flow as a function of the direction of wave propagation.

The incident energy is partly transmitted into plate j; the corresponding energy flow $\mathrm{d}\Pi_{ij}$ from plate i to plate j is given by

$$\mathrm{d}\Pi_{ij} = \tau_{ij}(\theta) l_{ij}\, \mathrm{d}I_x. \tag{28}$$

The total energy flow from plate i to plate j is calculated by integrating over all angles of incidence:

$$\Pi_{ij} = \frac{l_{ij}}{2\pi} \int_{-\pi/2}^{\pi/2} I_{xij}(\theta) D_i(\theta)\, \mathrm{d}\theta. \tag{29}$$

Finally the coupling loss factor can be calculated from the transmission coefficient by combining the SEA expression (21) with the result from the wave analysis, expression (29):

$$\eta_{ij} = \frac{2l_{ij}}{\omega^3 \pi M_i} \int_{0}^{\pi/2} I_{xij}(\theta) D_i(\theta)\, \mathrm{d}\theta. \tag{30}$$

Here, as stated before, the transmitted intensity I_{xij} has been calculated for an incident bending wave with unit amplitude.

4.2. MODAL DENSITY

The second topic concerns the calculation of the modal density of an orthotropic plate. This parameter enters, for instance, in the frequently used SEA reciprocity relation

$$n_i \eta_{ij} = n_j \eta_{ji}, \tag{31}$$

where n_i is the modal density of plate i for a given frequency. The total number of eigenmodes up to a certain frequency can be derived by means of the modal lattice shown in Figure 5, where each lattice point represents one eigenmode. The bending

wavenumber is plotted as a function of the angle of wave propagation θ for a certain frequency. The mode count can be evaluated as the ratio of the area enclosed by the wavenumber curve and the co-ordinate axes to the elementary area π^2/L_xL_y. For an orthotropic plate, the total number of eigenmodes up to a frequency f is given by

$$N(f)=\frac{f\sqrt{\rho h}S}{\pi}\int_0^{\pi/2}\frac{\mathrm{d}\theta}{\sqrt{B(\theta)}}. \tag{32}$$

Consequently, the modal density for bending waves on an orthotropic plate is the frequency independent value

$$n(f)=\frac{\mathrm{d}N(f)}{\mathrm{d}f}=\frac{\sqrt{\rho h}S}{\pi}\int_0^{\pi/2}\frac{\mathrm{d}\theta}{\sqrt{B(\theta)}}. \tag{33}$$

Lyon [16] replaced the integral by an average over the two stiffnesses in the principal directions. This approximation results in

$$n(f)\approx\frac{\sqrt{\rho h}S}{4}\left(\frac{1}{\sqrt{B_x}}+\frac{1}{\sqrt{B_y}}\right). \tag{34}$$

4.3. RECIPROCITY

Finally, it remains to be checked whether the reciprocity relation (31) is satisfied when the coupling loss factor and the modal density are calculated as explained in sections 4.1 and 4.2, respectively. From a closed form solution for the transmission coefficient of a symmetric cross-junction between isotropic plates, Kihlman [17] demonstrated the following reciprocity relation for the reversal of the transmission path:

$$\tau_{ij}(\theta_i)=\tau_{ji}(\theta_j). \tag{35}$$

The angles of propagation θ_i and θ_j are related by Snell's law:

$$k_{bi}(\theta_i)\sin(\theta_i)=k_{bj}(\theta_j)\sin(\theta_j). \tag{36}$$

Results of numerical calculations demonstrate that the reciprocity relation (35) is equally valid for the bending wave transmission coefficient of a junction between orthotropic plates. If this result is combined with expressions (30) and (33) for the coupling loss factor and the modal density, it can be verified that the SEA reciprocity relation (31) is satisfied.

5. NUMERICAL RESULTS

Results are presented for the case of a rigid L-junction of two identical orthotropic plates with the following dimensions and material properties: $h=0{\cdot}1$ m, $L_x=4{\cdot}0$ m, $L_y=4.{\cdot}0$ m, $E_x=4{\cdot}0\times10^{10}$ Pa, $E_y=2{\cdot}0\times10^{10}$ Pa, $G_{xy}=1{\cdot}154\times10^{10}$ Pa, $\nu_{xy}=0{\cdot}3$, $\rho=2500$ kg/m^3, $\eta_d=0{\cdot}01$.

The calculations with the model for finite-sized plates were carried out in small frequency steps for 50 randomly chosen excitation positions. The resulting velocity levels were then averaged over one-third octave bands and over all excitation positions. In all simulations, both plate edges parallel to the junction line are assumed to be free.

Four different types of L-junctions are considered, depending on the orientation of the plates. In Figure 7 the L-junctions are schematically indicated. The arrows on each plate indicate the stiffest principal material direction. In cases I and IV the plates have identical

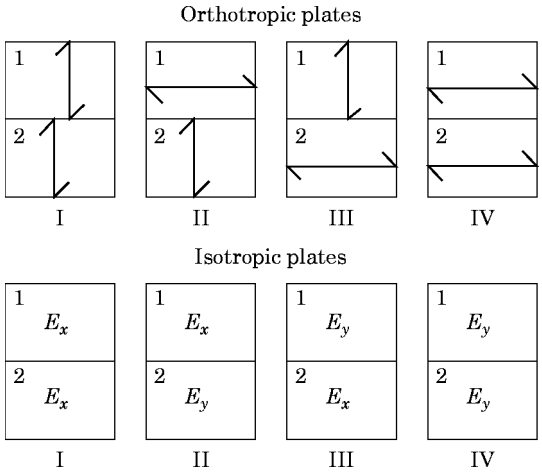

Figure 7. Four different L-junctions of orthotropic plates corresponding to four different cases of plate orientation.

orientations, whereas in cases II and III the plates have different orientations. Plate 1 is the source plate in all cases.

The bending wave transmission for a rigid L-junction of isotropic plates was also calculated in order to find an isotropic equivalent for a junction between orthotropic plates. For the case of similarly oriented plates, the Young's modulus of the isotropic plate corresponds to the Young's modulus of the orthotropic plate in the direction normal to the junction line. For the case of dissimilar plate orientation it is the Young's modulus parallel to the junction line that determines the Young's modulus of the corresponding isotropic plate. In the equivalent isotropic junctions in Figure 7, E_x represents the Young's modulus of the stiffest direction of the corresponding orthotropic plate.

Figure 8(a) shows the bending wave transmission loss for the four different plate orientations. It is clearly shown that the model for semi-infinite plates is not very sensitive to the Young's modulus of the plates. All curves lie within a range of 1 dB.

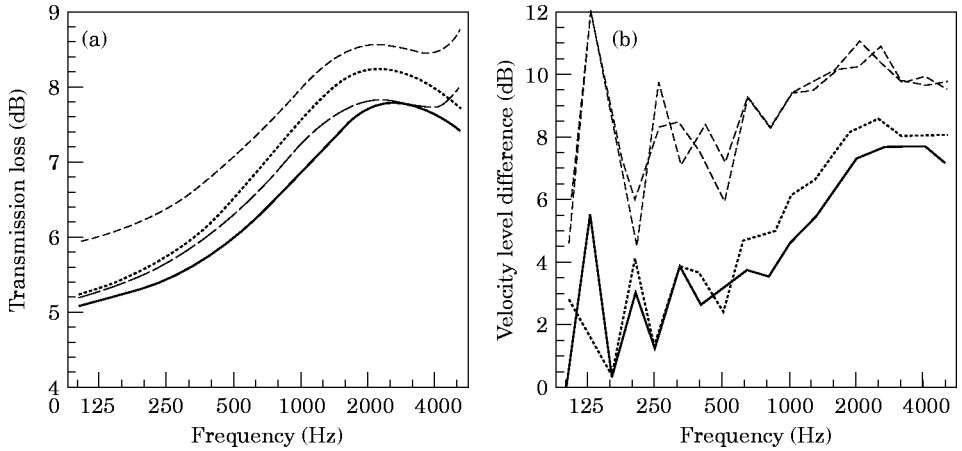

Figure 8. Transmission loss for an L-junction of two semi-infinite orthotropic plates (a) and velocity level difference for an L-junction of two finite orthotropic plates (b) for four plate orientations: case I (——); case II (– –); case III (- - - -); case IV (· · · · · · ·).

Figure 8(b) shows the transverse velocity level difference for the case of an L-junction of finite-sized orthotropic plates. For this model, there is a significant difference between the cases of similar and dissimilar orientation. The lowest level difference is obtained for the similarly oriented plates, whereas a more efficient attenuation is predicted for the plates with dissimilar orientation. This result can be explained by starting from the fact that the energy exchange between the two plates is most efficient when their mode shapes and eigenfrequencies match. In the example, both plates are square and have identical thickness and material properties, and consequently all eigenfrequencies match perfectly regardless of mutual plate orientation. In the cases of dissimilar orientation, however, there are fewer mode shapes that spatially match along the junction line. The limited number of modes participating at the vibration transmission for the case of dissimilar orientation also explains the more irregular level difference at low frequencies compared to that for the case of similar orientation. For higher frequencies or higher modal densities, the number of modes and their spatial matching become increasingly similar for both cases, and the differences in sound transmission gradually level out.

In Figures 9 and 10 the results for the equivalent junction of isotropic plates are compared to the results for the junction of orthotropic plates. The results of the model for semi-infinite plates show very good agreement, as could be expected from its low sensitivity to the Young's modulus. For the model for finite plates the agreement is less, but still reasonable. For this junction, the maximum differences amount to 3 dB for the cases of dissimilar orientation. From the results of similar calculations we concluded that a stiffness ratio of 5 is the limit for an acceptable agreement. This limit is most critical for cases II, III and IV of plate orientation, and the average difference between isotropic and orthotropic results amounts to 2 dB with a standard deviation of 3 dB. However, for case IV the differences can become higher than 10 dB at low frequencies. This can be explained by the fact that the equivalent isotropic plates are characterized by a considerably higher modal density than the corresponding orthotropic plates. These results suggest that bending wave transmission between moderately orthotropic plates can be calculated with reasonable accuracy by means of an isotropic plate model.

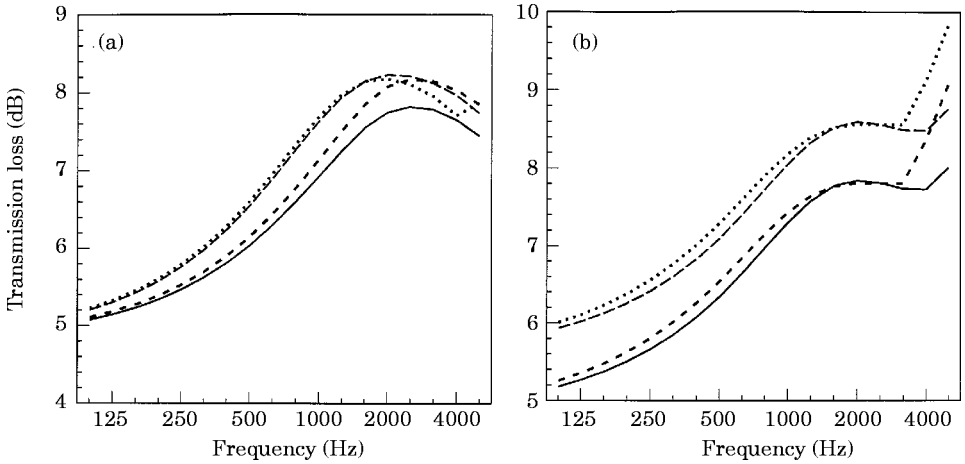

Figure 9. Comparison between the orthotropic L-junction and the equivalent isotropic L-junction of semi-infinite plates. (a) Similar plate orientation: orthotropic plates: case I (——), case IV (– –); isotropic plates: case I (- - - -), case IV: (· · · · · · ·). (b) Dissimilar plate orientation: orthotropic plates: case II (——), case III (– –); isotropic plates: case II (- - - -), case III: (· · · · · · ·).

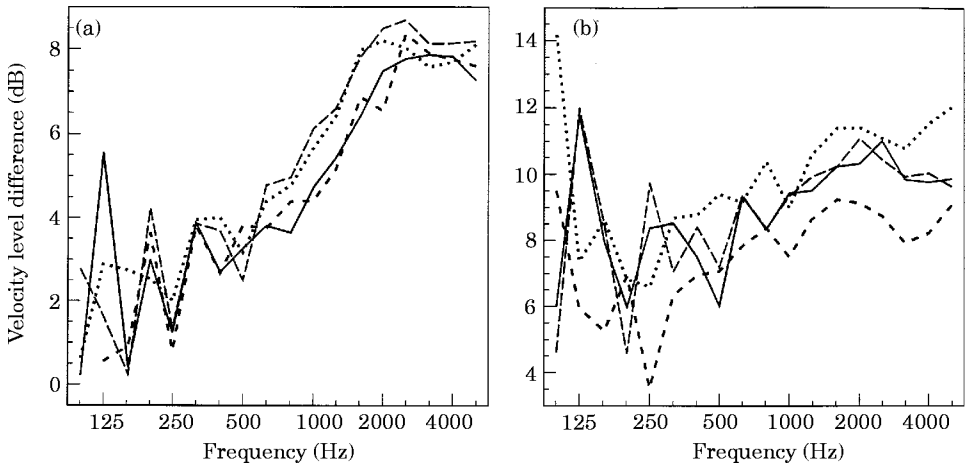

Figure 10. Comparison between the orthotropic L-junction and the equivalent isotropic L-junction of finite places. (a) Similar plate orientation: orthotropic plates: case I (——), case IV (– –); isotropic plates: case I (- - - -), case IV: (· · · · · · ·). (b) Dissimilar plate orientation: orthotropic plates: case II (——), case III (– –); isotropic plates: case II (- - - -), case III: (· · · · · · ·).

To compare further the results of the models for infinite and finite plates, coupling loss factors calculated from the transmission coefficient of the semi-infinite plate junction were introduced into a simple two-subsystem SEA [16] model. The energy of the subsystems is the total kinetic energy of the bending waves of the plates. Since both plates of the junction have identical mass, the energy level difference of the plates equals their transverse velocity level difference. Figure 11 compares the results of the SEA model to the results of the finite-plate model. For the cases of similar orientation results of the SEA model correspond well to results of the model for finite-sized plates. For cases II and III, however, the SEA model clearly overestimates the bending wave transmission. A possible explanation for this phenomenon is provided by the different types of coupling considered by the two models. When studying the energy flow between two plates, the finite plate

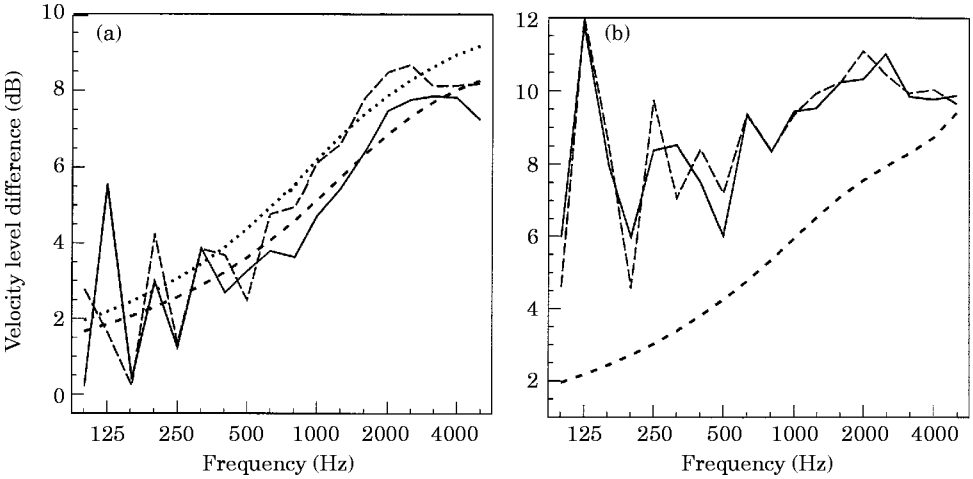

Figure 11. Comparison between SEA and finite plate calculations for an L-junction of two finite orthotropic plates. (a) Similar plate orientation: finite plate model: case I (——), case IV (– –); SEA model: case I (- - - -), case IV (· · · · · · ·). (b) Dissimilar plate orientation: finite plate model: case II (——), case III (– –); SEA model: cases II and III (- - - -).

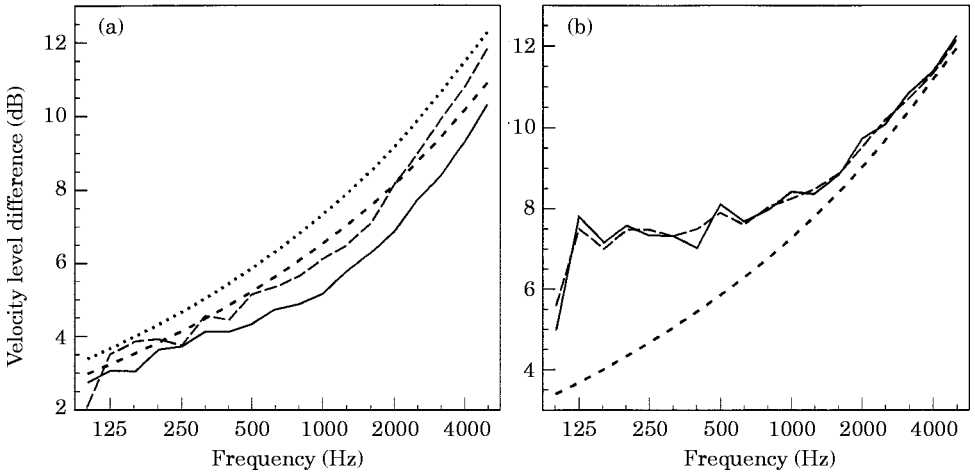

Figure 12. Comparison between SEA and finite plate calculations for an L-junction of two finite orthotropic plates with decreased thickness ($h = 0{\cdot}02$ m). (a) Similar plate orientation: finite plate model: case I (——), case IV (– –); SEA model: case I (- - - -), case IV (· · · · · · ·). (b) Dissimilar plate orientation: finite plate model: case II (——), case III (– –); SEA model: cases II and III (- - - -).

model predicts the actual coupling between the eigenmodes, where the SEA model assumes that, in a certain frequency interval, every mode of the first plate is evenly coupled to every mode of the second plate. However, when the eigenmodes have very different shapes, this assumption ceases to be valid, except for higher modal densities of the plates. To illustrate this, we increased the modal density of the plates by reducing their thickness to 0·02 m. Again, for the case of identically oriented plates a very good agreement is achieved between both calculation methods (see Figure 12(a)). The results in Figure 12(b) show that the difference between the results of the finite plate model and the SEA calculation gradually decreases from 4 dB to zero with increasing frequency. This better agreement is caused by the improvement of the coupling between the modes of the dissimilarly oriented plates, resulting in a decreased bending wave attenuation. From these results we could conclude that, apart from dimensions and material properties, the mutual plate orientation supplies us with an extra tool in controlling bending wave transmission in a structure consisting of orthotropic plates. However, experimental research should be performed in order to validate the practical significance of these calculations.

6. CONCLUSIONS

The bending wave transmission between thin orthotropic plates has been studied for the case of a junction of semi-infinite plates and for the case of a junction of finite-sized plates. The influence of the mechanical behaviour of orthotropic plates on the wave propagation has been investigated. Calculations of the bending wave transmission at the L-junction of orthotropic plates illustrate the very low sensitivity to the Young's modulus of the model for semi-infinite plates. The model for the finite plates predicts a more efficient bending wave attenuation for the cases of dissimilar plate orientation. For both models, however, calculations for the case of an equivalent L-junction of isotropic plates show good agreement with the results for the junction of orthotropic plates. This leads to the conclusion that in building acoustics the estimation of bending wave transmission can very well be performed with a model for isotropic plates without making a significant error, even if the bending stiffness in one principal direction is twice the bending stiffness

in the other principal direction. Finally, calculation results have demonstrated the importance of the mutual plate orientation in the bending wave transmission between orthotropic plates.

ACKNOWLEDGMENTS

This research was funded by a grant from the Flemish Institute for the Promotion of Scientific Technological Research in Industry (IWT).

REFERENCES

1. J. L. Guyader, C. Boisson and C. Lesueur 1982 *Journal of Sound and Vibration* **81**(1), 81–92. Energy transmission in finite coupled plates, part I: theory.
2. Y. Shen and B. M. Gibbs 1986 *Journal of Sound and Vibration* **105**(1), 73–90. An approximate solution for the bending vibrations of a combination of rectangular thin plates.
3. C. Simmons 1991 *Journal of Sound and Vibration* **144**(2), 215–227. Structure-borne sound transmission through plate junctions and estimates of SEA coupling loss factors using the finite element method.
4. C. R. Fredö 1993 *Licentiate of Engineering Thesis*, *Chalmers University of Technology Report* F 93-01. Derivation of energy flow with a finite element model.
5. M. D. McCollum and J. M. Cuschieri 1990 *Journal of the Acoustical Society of America* **88**(3), 1472–1479. Thick plate bending wave transmission using a mobility power flow approach.
6. R. S. Langley and K. H. Heron 1990 *Journal of Sound and Vibration* **143**(2), 241–253. Elastic wave transmission through plate-beam junctions.
7. L. Cremer, M. Heckl and E. E. Ungar 1988 *Structure-Borne Sound*. Berlin: Springer Verlag; second edition.
8. W. Wöhle, Th. Beckmann and H. Schreckenbach 1981 *Journal of Sound and Vibration* **77**, 323–337. Coupling loss factors for statistical energy analysis of sound transmission at rectangular structural slab joints, part I.
9. W. Wöhle, Th. Beckmann and H. Schreckenbach 1981 *Journal of Sound and Vibration* **77**, 335–344. Coupling loss factors for statistical energy analysis of sound transmission at rectangular structural slab joints, part II.
10. P. Mees and G. Vermeir 1993 *Journal of Sound and Vibration* **166**(1), 55–76. Structure-borne sound transmission at elastically connected plates.
11. P. Mees and G. Vermeir 1993 *Proceedings Inter-noise 93*, 457–462. Structure-borne sound transmission at elastically coupled plates.
12. R. M. Jones 1975 *Mechanics of Composite Materials*. New York: McGraw-Hill.
13. P. G. Craven and B. M. Gibbs 1981 *Journal of Sound and Vibration* **77**, 417–427. Sound transmission and mode coupling at junctions of thin plates, part I: representation of the problem.
14. B. M. Gibbs and P. G. Craven 1981 *Journal of Sound and Vibration* **77**, 429–435. Sound transmission and mode coupling at junctions of thin plates, part II: parametric survey.
15. J. M. Cuschieri 1990 *Journal of the Acoustical Society of America* **87**(3), 1159–1165. Stuctural power-flow analysis using a mobility power flow approach of an L-shaped plate.
16. R. H. Lyon 1975 *Statistical Energy Analysis of Dynamic Systems*. Cambridge, Massachusetts: MIT Press.
17. T. Kihlman 1967 *Transmission of structure-borne sound through buildings*. Report 9, National Swedish Institute for Building Research.

APPENDIX: LIST OF SYMBOLS

$A, B, C, D,$ A', B', C', D'	eigenmode amplitudes
B_i	bending stiffness in direction i
C_g	group velocity
D_i	weighting function for the power distribution in a diffuse field on plate i.
E	Young's modulus
E'	Young's modulus for plane stress condition

E_{di}	kinetic energy per unit area on plate i
E_{ki}	total kinetic energy on plate i
f	frequency
F_x, F_y, F_z	forces per unit width in x-, y- and z-directions
G	shear modulus
h	plate thickness
I	intensity
k_b	bending wavenumber
k_p	in-plane wavenumber
l_{ij}	coupling length between plate i and plate j
L_x, L_y	dimensions of the plate
L_{vp}	velocity level difference between plate 1 and plate p
M_i	total mass of plate i
M_y	bending moment per unit width around y-axis
n	modal density
N	mode count
R_p	bending wave transmission loss
S_i	total area of plate i
t	time
V	in-plane translation ratio
x, y, z	co-ordinates, x- and y-directions parallel to the first and second principal material directions of the plate
ξ	displacement along x-axis
η	displacement along y-axis
ζ	displacement around z-axis
α_y	rotation around y-axis
γ	shear strain
η_d	internal damping
η_{ij}	coupling loss factor from subsystem i to subsystem j
ϵ	normal strain
θ	angle with x-axis
v	Poisson's ratio
Π_{ij}	total energy flow from subsystem i to subsystem j
ρ	density of the plate material
σ	normal stress
τ	shear stress
τ_{ij}	transmission ratio from plate i to plate j
$\bar{\tau}_p$	bending wave transmission ratio for random incidence
ω	circular frequency

Subscripts

0	referring to junction beam
1	referring to plate 1
x, y, z	referring to x-, y- and z-axis, respectively
n	referring to mode number
p	referring to plate p